University of South Carolina
Scholar Commons

Faculty Publications | Chemical Engineering, Department of

1987

A Mathematical Model of a Lead-Acid Cell: Discharge, Rest, and Charge

Hiram Gu

T. V. Nguyen

Ralph E. White
University of South Carolina - Columbia, white@cec.sc.edu

Follow this and additional works at: https://scholarcommons.sc.edu/eche_facpub

 Part of the Chemical Engineering Commons

Publication Info

Journal of the Electrochemical Society, 1987, pages 2953-2960.
© The Electrochemical Society, Inc. 1987. All rights reserved. Except as provided under U.S. copyright law, this work may not be reproduced, resold, distributed, or modified without the express permission of The Electrochemical Society (ECS). The archival version of this work was published in the Journal of the Electrochemical Society.
http://www.electrochem.org/
DOI: 10.1149/1.2100322
http://dx.doi.org/10.1149/1.2100322

This Article is brought to you by the Chemical Engineering, Department of at Scholar Commons. It has been accepted for inclusion in Faculty Publications by an authorized administrator of Scholar Commons. For more information, please contact dillarda@mailbox.sc.edu.

The independent sizing of the redox system's power and storage capacity makes it particularly attractive for long term electricity storage in remote areas where solar arrays or wind generators have been installed. An attractive feature of the vanadium redox battery is that since there is no solution contamination due to cross-mixing, after the original capital investment, there would be negligible running and maintenance costs. Since the cell can be completely discharged without any deterioration in performance, it would be ideally suited for large scale energy storage in load leveling applications.

A larger scale five-cell battery unit is currently under construction so that the system performance can be further tested before scaling up to a 1 kW unit.

Acknowledgments

Support for this project was provided under the National Energy Research Development and Demonstration Programme which is administered by the Australian Commonwealth Department of Resources and Energy. The authors are grateful to Dr. Miron Rychcik for useful discussions.

Manuscript submitted Sept. 2, 1986; revised manuscript received Dec. 16, 1986.

The University of New South Wales assisted in meeting the publication costs of this article.

REFERENCES

1. L. H. Thaller, NASA TMX-71540, National Aeronautics and Space Administration, U.S. Department of Energy, 1974; and U.S. Pat. 3,996,064 (1974).
2. L. H. Thaller, NASA TMM-79143, National Aeronautics and Space Administration, U.S. Department of Energy, 1979.
3. Redox Flow Cell Development and Demonstration Project, NASA TM-79067, National Aeronautics and Space Administration, U.S. Dept. of Energy, 1979.
4. H. H. Hagedorn and L. H. Thaller, NASA TM-81464, National Aeronautics and Space Administration, U.S. Department of Energy, 1980.
5. D. A. Johnson and M. A. Reid, NASA TM-82913, National Aeronautics and Space Administration, U.S. Department of Energy, 1982.
6. K. Nozaki, H. Kaneko, A. Negishi, and T. Ozawa, in "Proceedings of Meeting" pp. 1641-1646, 18th IECEC (1983).
7. R. F. Gahn, N. H. Hagedorn, and J. A. Johnson, NASA TM87034, National Aeronautics and Space Administration, U.S. Department of Energy, 1985.
8. M. Skyllas-Kazacos, M. Rychcik, and R. Robins, Patent Applications filed.
9. M. Skyllas-Kazacos, M. Rychcik, R. Robins, A. Fane, and M. Green, *This Journal*, **133**, 1057 (1986).
10. R. Rychcik and M. Skyllas-Kazacos, *J. Power Sources*, **19**, 45 (1986).
11. D.-G. Oei, *J. Appl. Electrochem.*, **15**, 231 (1985).

A Mathematical Model of a Lead-Acid Cell

Discharge, Rest, and Charge

Hiram Gu* and T. V. Nguyen,,[1]**

Electrochemistry Department, General Motors Research Laboratories, Warren, Michigan 48090-9055

R. E. White*

Department of Chemical Engineering, Texas A&M University, College Station, Texas 77843-3122

ABSTRACT

A mathematical model of a lead-acid cell is presented which includes the modeling of porous electrodes and various physical phenomena in detail. The model is used to study the dynamic behavior of the acid concentration, the porosity of the electrodes, and the state of charge of the cell during discharge, rest, and charge. The dependence of the performance of the cell on electrode thicknesses and operating temperature is also investigated.

The lead-acid system is used in the largest number of secondary batteries manufactured in the world. The most important market remains the car battery for starting, lighting, and ignition, with approximately 50×10^6 units sold per year in the U.S.A. (1). Other applications are in emergency power supplies, load-leveling, and more recently for instruments, radio, and other electrical apparatus. The design and improvement of these batteries are mostly done by trial-and-error.

This traditional approach, which consists of experimental cell build-ups and extensive testing, is costly and time consuming. Furthermore, results from such tests provide only global information and do not provide insight into the governing phenomena. It is advantageous to develop a mathematical model of the cell which would allow one to gain a better understanding of the cause and effect relationships and the phenomena involved, and suggest directions for improvements.

Complementing experimental testing with mathematical modeling is a cost effective approach to the development and design of batteries. Testing is still needed to verify predictions of the model and to uncover physical phenomena that may not have been included in the model. But with the help of this mathematical tool, extensive experimental testing is no longer needed. Great savings in material, labor, and time can be realized in the development of a new battery.

The first use of mathematical models to describe the behavior of the lead-acid system was applied to the porous positive electrode (PbO_2) by Stein (2, 3) and Euler (4), with further improvements made by Simonsson (5-7), Micka and Rousar (8), Gidaspow and Baker (9), and others. A good review of the development in the theory of flooded porous electrodes prior to 1975 has been provided by Newman and Tiedemann (10). Recently, Tiedemann and Newman (11) and Sunu (12) applied Newman's theory to the development of a complete cell model describing the discharge behavior of the lead-acid battery system. However, a model for predicting the cell behavior during charge and rest, as well as the effects of cycling, is not available. To assist designers and engineers in the further development of the lead-acid batteries with improved performance and cycle life, a detailed mathematical model of a lead-acid cell is presented that can be used to predict the dynamic behavior of the cell not only during discharge, but also during charge, rest, and cycling.

Model Development

A schematic for the lead-acid cell is shown in Fig. 1. The cell consists of the following boundaries and re-

*Electrochemical Society Active Member.
**Electrochemical Society Student Member.
[1]Present address: Department of Chemical Engineering, Texas A&M University, College Station, Texas 77843-3122.

Downloaded 13 Jun 2011 to 129.252.106.227. Redistribution subject to ECS license or copyright; see http://www.ecsdl.org/terms_use.jsp

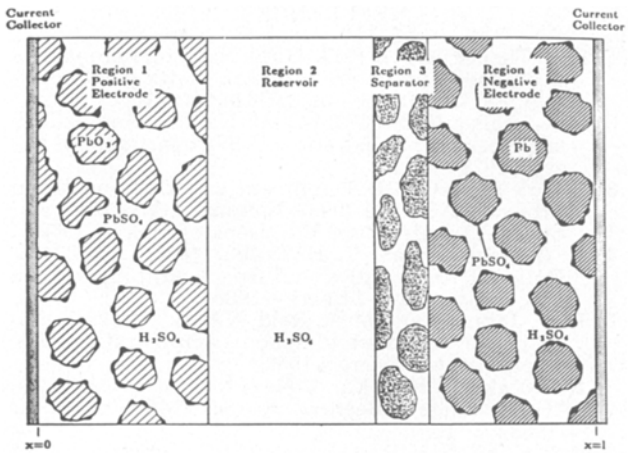

Fig. 1. One-dimensional macro-homogeneous model of a lead-acid cell

gions: a lead grid current collector at $x = 0$, which is at the center of the positive electrode, the positive (PbO_2) electrode (region 1), the positive electrode/reservoir interface, the reservoir (region 2), the reservoir/separator interface, the separator (region 3), the separator/negative electrode interface, the negative (Pb) electrode (region 4), and the center of the negative electrode where another grid is located. Details of the geometry are ignored and the whole cell is regarded as a homogeneous macroscopic entity with distributed quantities in the direction perpendicular to the grid. An extensive discussion of average quantities used in the development of the model has been given by Dunning (13) and Trainham (14). Additionally, isothermal conditions are assumed here. The electrolyte is concentrated H_2SO_4 which is considered to be a binary electrolyte that dissociates into H^+ and HSO_4^- in H_2O.

The electrode reactions during discharge are

$$PbO_{2(s)} + HSO_4^- + 3H^+ + 2e^- \xrightarrow{\text{discharge}} PbSO_{4(s)} + 2H_2O$$

(positive electrode)

and

$$Pb_{(s)} + HSO_4^- \xrightarrow{\text{discharge}} PbSO_{4(s)} + 2e^- + H^+$$

(negative electrode)

There are five explicit unknowns in the model: acid concentration (c), electrode porosity (ϵ), superficial current density in the electrolyte (i_2), potential in the solid phase (ϕ_1), and potential in the electrolyte (ϕ_2). The governing equations and boundary conditions are presented next.

Center of the positive electrode, $x = 0$.—

$$\frac{\partial c}{\partial x} = 0 \quad [1]$$

$$\frac{\partial \epsilon}{\partial x} = 0 \quad [2]$$

$$i_2 = 0 \quad [3]$$

$$\phi_1 = 0 \quad [4]$$

$$\frac{\partial \phi_2}{\partial x} = 0 \quad [5]$$

Equations [1], [2], and [5] are in accordance with the assumption of symmetry. Equation [3] states that, at the center of the positive electrode, all the current is in the current collector and none is in the electrolyte. In Eq. [4], as a convenient choice, the solid phase potential, ϕ_1, is designated to be 0 V at this boundary. Without this reference potential, a particular solution cannot be obtained.

Region 1, positive electrode.—

porosity variation—

$$\frac{\partial \epsilon}{\partial t} - \frac{1}{2\mathbf{F}}\left(\frac{MW_{PbSO_4}}{\rho_{PbSO_4}} - \frac{MW_{PbO_2}}{\rho_{PbO_2}}\right)\frac{\partial i_2}{\partial x} = 0 \quad [6]$$

Ohm's law in solution—

$$\frac{i_2}{\epsilon^{ex1}\kappa} + \frac{\partial \phi_2}{\partial x} - \frac{RT}{\mathbf{F}}(1 - 2t^\circ_+)\frac{\partial \ln (cf)}{\partial x} = 0 \quad [7]$$

Ohm's law in solid—

$$i_2 - \epsilon^{exm1}\sigma_{PbO_2}\frac{\partial \phi_1}{\partial x} - I = 0 \quad [8]$$

material balance—

$$\epsilon\frac{\partial c}{\partial t} - \frac{1}{2\mathbf{F}}\left[\left(\frac{MW_{PbSO_4}}{\rho_{PbSO_4}} - \frac{MW_{PbO_2}}{\rho_{PbO_2}}\right) - (3 - 2t^\circ_+)\bar{V}_e + 2\bar{V}_o\right] i_2\frac{\partial c}{\partial x} - \frac{\partial}{\partial x}\left(\epsilon^{ex1} D\frac{\partial c}{\partial x}\right) - \left[\left(\frac{3 - 2t^\circ_+}{2\mathbf{F}}\right)(1 - c\bar{V}_e) + \frac{c\bar{V}_o}{\mathbf{F}}\right]\frac{\partial i_2}{\partial x} = 0 \quad [9]$$

electrode kinetics—for discharge and rest

$$\frac{\partial i_2}{\partial x} - a_{max1} i_{o1,ref}\left(\frac{c}{c_{ref}}\right)^{\gamma 1}\left(\frac{\epsilon - \epsilon_{o1}}{\epsilon_{max1} - \epsilon_{o1}}\right)^{\zeta 1}\left\{\exp\left[\frac{\alpha_{a1}\mathbf{F}}{RT}(\phi_1 - \phi_2 - U_{PbO_2})\right] - \exp\left[\frac{-\alpha_{c1}\mathbf{F}}{RT}(\phi_1 - \phi_2 - U_{PbO_2})\right]\right\} = 0 \quad [10a]$$

and for charge

$$\frac{\partial i_2}{\partial x} - a_{max1} i_{o1,ref}\left(\frac{c}{c_{ref}}\right)^{\gamma 1}\left(\frac{\epsilon - \epsilon_{o1}}{\epsilon_{max1} - \epsilon_{o1}}\right)^{\zeta 1}\left(\frac{\epsilon_{max1} - \epsilon}{\epsilon_{max1} - \epsilon_{o1}}\right)\left\{\exp\left[\frac{\alpha_{a1}\mathbf{F}}{RT}(\phi_1 - \phi_2 - U_{PbO_2})\right] - \exp\left[\frac{-\alpha_{c1}\mathbf{F}}{RT}(\phi_1 - \phi_2 - U_{PbO_2})\right]\right\} = 0 \quad [10b]$$

where

$$U_{PbO_2} \approx U_{PbO_2}{}^\theta - U_{Pb}{}^\theta \quad [11]$$

Equation [6] describes the change in porosity with time due to the conversion of the active material in the electrode reaction. Equation [7] is a modified Ohm's law for the electrolyte which states that the current in the electrolyte is driven by the electric potential and chemical potential gradients. Equation [8] is Ohm's law applied to the solid matrix. Equation [9] states that the electrolyte concentration at any point in space changes with time because of the electrode reaction, diffusion, and migration. Equations [10a] and [10b] are kinetic expressions for the electrode reaction. Equation [10b] includes a factor to account for the depletion of lead sulfate as lead dioxide is being formed. For convenience, the dependence of the overpotential on the acid concentration is neglected, and a concentration independent lead electrode is used as a reference electrode in Eq. [10a], [10b], and [11].

Interface between region 1 and 2.—

$$\epsilon^{ex1}\left.\frac{\partial c}{\partial x}\right|_{region\ 1} = \left.\frac{\partial c}{\partial x}\right|_{region\ 2} \quad [12]$$

$$\frac{\partial \epsilon}{\partial t} - \frac{1}{2\mathbf{F}}\left(\frac{MW_{PbSO_4}}{\rho_{PbSO_4}} - \frac{MW_{PbO_2}}{\rho_{PbO_2}}\right)\frac{\partial i_2}{\partial x} = 0 \quad [13]$$

Downloaded 13 Jun 2011 to 129.252.106.227. Redistribution subject to ECS license or copyright; see http://www.ecsdl.org/terms_use.jsp

$$i_2 = I \quad [14]$$

$$\left.\frac{\partial \phi_1}{\partial x}\right|_{\text{region 1}} = 0 \quad [15]$$

$$\epsilon^{\text{ex1}} \left.\frac{\partial \phi_2}{\partial x}\right|_{\text{region 1}} = \left.\frac{\partial \phi_2}{\partial x}\right|_{\text{region 2}} \quad [16]$$

Equations [12] and [16] satisfy the requirement that the flux of a species i, N_i, and the superficial current density, i_2, are continuous across the interface. In other words, $N_{i,\text{region 1}} = N_{i,\text{region 2}}$ and $i_{2,\text{region 1}} = i_{2,\text{region 2}}$; with $i = +, -$, or o. But since [Ref. (15)]

$$v^{\blacksquare} = \sum_i c_i v_i \bar{V}_i \quad [17]$$

and

$$N_i = c_i v_i \quad [18]$$

with $\bar{V}_i$ assumed constant, the requirement that the flux of species i is continuous implies that the volume average velocity is also continuous, *i.e.*, $v_1^{\blacksquare} = v_2^{\blacksquare}$.

Equation [13] describes the porosity variation with time and Eq. [14] states that all the current at the interface is in the electrolyte phase. Finally, Eq. [15] states that the electrode solid phase potential gradient is equal to zero at the interface because the electrode solid phase ends there.

Region 2, reservoir.—

porosity—

$$\epsilon = 1 \quad [19]$$

Ohm's law in solution—

$$\frac{i_2}{\kappa} + \frac{\partial \phi_2}{\partial x} - \frac{RT}{\mathbf{F}}(1 - 2t^\circ_+)\frac{\partial \ln (cf)}{\partial x} = 0 \quad [20]$$

solid phase potential—

$$\phi_1 = 0 \quad [21]$$

material balance—

$$\frac{\partial c}{\partial t} - \frac{1}{2\mathbf{F}}\left[\left(\frac{MW_{\text{PbSO}_4}}{\rho_{\text{PbSO}_4}} - \frac{MW_{\text{PbO}_2}}{\rho_{\text{PbO}_2}}\right) - (3 - 2t^\circ_+)\bar{V}_e + 2\bar{V}_o\right] I \frac{\partial c}{\partial x} - D\frac{\partial^2 c}{\partial x^2} = 0 \quad [22]$$

current in solution—

$$i_2 = I \quad [23]$$

Equation [19] states that the reservoir is filled with electrolyte. Equation [20] is Ohm's law applied to the electrolyte written with respect to Pb reference electrode. The electrode solid phase potential is zero (Eq. [21]) because there is no electrode solid phase in the reservoir. Equation [22] is the material balance for the electrolyte in the reservoir. Finally, Eq. [23] states that all the applied current is flowing through the solution phase since there is no electrode solid phase in the reservoir.

Interface between region 2 and region 3.—

$$D\left.\frac{\partial c}{\partial x}\right|_{\text{region 2}} - cv_2^{\blacksquare} = D\epsilon_{\text{sep}}^{\text{ex3}}\left.\frac{\partial c}{\partial x}\right|_{\text{region 3}} - cv_3^{\blacksquare} \quad [24]$$

where

$$v_2^{\blacksquare} = -\frac{1}{2\mathbf{F}}\left[\left(\frac{MW_{\text{PbSO}_4}}{\rho_{\text{PbSO}_4}} - \frac{MW_{\text{PbO}_2}}{\rho_{\text{PbO}_2}}\right) - (3 - 2t^\circ_+)\bar{V}_e + 2\bar{V}_o\right] I$$

$$v_3^{\blacksquare} = \frac{1}{2\mathbf{F}}\left[\left(\frac{MW_{\text{PbSO}_4}}{\rho_{\text{PbSO}_4}} - \frac{MW_{\text{Pb}}}{\rho_{\text{Pb}}}\right) + (1 - 2t^\circ_+)\bar{V}_e\right] I$$

$$\epsilon = \epsilon_{\text{sep}} \quad [25]$$

$$i_2 = I \quad [26]$$

$$\phi_1 = 0 \quad [27]$$

$$\left[\frac{\partial \phi_2}{\partial x} - \frac{RT}{\mathbf{F}}(1 - 2t^\circ_+)\frac{\partial \ln (cf)}{\partial x}\right]_{\text{region 2}} = \left[\epsilon_{\text{sep}}^{\text{ex3}}\frac{\partial \phi_2}{\partial x} - \epsilon_{\text{sep}}^{\text{ex3}}\frac{RT}{\mathbf{F}}(1 - 2t^\circ_+)\frac{\partial \ln (cf)}{\partial x}\right]_{\text{region 3}} \quad [28]$$

Equation [24] satisfies the condition that the fluxes of the species are continuous. As shown by the expressions for $v_2^{\blacksquare}$ and $v_3^{\blacksquare}$ below Eq. [24], $v_2^{\blacksquare}$ is not equal to $v_3^{\blacksquare}$. $v_2^{\blacksquare}$ is equal to $v_1^{\blacksquare}$ as stated earlier and $v_3^{\blacksquare}$ is equal to $v_4^{\blacksquare}$ which is the volume average velocity due to migration and changes in the structure of the lead electrode (*i.e.*, region 4). The implicit requirement that $v_2^{\blacksquare} = v_3^{\blacksquare}$ is not met here. This inconsistency would be removed in a two-dimensional model which included the fact that the level of the acid changes during charge and discharge. Previous workers (11, 16, 17) have avoided this problem by assuming that the reservoir is well mixed and, consequently, separates the convective flows out of (or into) the porous electrodes. Since the magnitudes of the volume average velocities are typically small, this inconsistency is ignored in the model presented here.

Equation [25] sets the porosity at this interface to be that of the separator porosity, which is a constant value. Equation [26] indicates that the superficial current density in the solution is equal to the applied current density since no charge transfer reaction occurs in either the reservoir or the separator. Equation [27] sets the electrode solid phase potential to zero since there is no electrode here. Equation [28] satisfies the condition that the current is continuous across the interface. Unlike Eq. [16] where the terms with the concentration gradients cancel according to Eq. [12], the concentration gradient terms in Eq. [28] do not cancel because they are not equal according to Eq. [24].

Region 3, separator.—

porosity—

$$\epsilon = \epsilon_{\text{sep}} \quad [29]$$

Ohm's law in solution—

$$\frac{i_2}{\epsilon_{\text{sep}}^{\text{ex3}}\kappa} + \frac{\partial \phi_2}{\partial x} - \frac{RT}{\mathbf{F}}(1 - 2t^\circ_+)\frac{\partial \ln (cf)}{\partial x} = 0 \quad [30]$$

solid phase potential—

$$\phi_1 = 0 \quad [31]$$

material balance—

$$\epsilon_{\text{sep}}\frac{\partial c}{\partial t} + \frac{1}{2\mathbf{F}}\left[\left(\frac{MW_{\text{PbSO}_4}}{\rho_{\text{PbSO}_4}} - \frac{MW_{\text{Pb}}}{\rho_{\text{Pb}}}\right) + (1 - 2t^\circ_+)\bar{V}_e\right] I \frac{\partial c}{\partial x} - \epsilon_{\text{sep}}^{\text{ex3}} D\frac{\partial^2 c}{\partial x^2} = 0 \quad [32]$$

current in solution—

$$i_2 = I \quad [33]$$

Equation [32] is the material balance for the electrolyte in the separator. The second term in the equation is $v_3^{\blacksquare}(\partial c/\partial x)$, where $v_3^{\blacksquare}$ is equal to that at the interface of regions 3 and 4. The porosity of the separator is fixed (Eq. [29]), and the current density in the solution is equal to the applied current density (Eq. [33]). The electrode solid phase potential again is set to zero because there is no electrode here (Eq. [31]). Finally, Eq. [30] is Ohm's law applied to the solution phase in the separator.

Interface between region 3 and region 4.—

$$\epsilon_{\text{sep}}^{\text{ex3}}\left.\frac{\partial c}{\partial x}\right|_{\text{region 3}} = \epsilon^{\text{ex4}}\left.\frac{\partial c}{\partial x}\right|_{\text{region 4}} \quad [34]$$

Downloaded 13 Jun 2011 to 129.252.106.227. Redistribution subject to ECS license or copyright; see http://www.ecsdl.org/terms_use.jsp

$$\frac{\partial \epsilon}{\partial t} + \frac{1}{2\mathbf{F}}\left(\frac{MW_{PbSO_4}}{\rho_{PbSO_4}} - \frac{MW_{Pb}}{\rho_{Pb}}\right)\frac{\partial i_2}{\partial x} = 0 \quad [35]$$

$$i_2 = I \quad [36]$$

$$\left.\frac{\partial \phi_1}{\partial x}\right|_{\text{region 4}} = 0 \quad [37]$$

$$\epsilon_{sep}^{ex3}\left.\frac{\partial \phi_2}{\partial x}\right|_{\text{region 3}} = \epsilon^{ex4}\left.\frac{\partial \phi_2}{\partial x}\right|_{\text{region 4}} \quad [38]$$

The equations for this interface were established with the same reasoning that was used for the interface between region 1 and region 2.

Region 4, negative electrode.—

porosity variation—

$$\frac{\partial \epsilon}{\partial t} + \frac{1}{2\mathbf{F}}\left(\frac{MW_{PbSO_4}}{\rho_{PbSO_4}} - \frac{MW_{Pb}}{\rho_{Pb}}\right)\frac{\partial i_2}{\partial x} = 0 \quad [39]$$

Ohm's law in solution—

$$\frac{i_2}{\epsilon^{ex4}\kappa} + \frac{\partial \phi_2}{\partial x} - \frac{RT}{\mathbf{F}}(1 - 2t^\circ_+)\frac{\partial \ln (cf)}{\partial x} = 0 \quad [40]$$

Ohm's law in solid—

$$i_2 - \epsilon^{exm4}\sigma_{Pb}\frac{\partial \phi_1}{\partial x} - I = 0 \quad [41]$$

material balance—

$$\epsilon\frac{\partial c}{\partial t} + \frac{1}{2\mathbf{F}}\left[\left(\frac{MW_{PbSO_4}}{\rho_{PbSO_4}} - \frac{MW_{Pb}}{\rho_{Pb}}\right) + (1 - 2t^\circ_+)\bar{V}_e\right] i_2\frac{\partial c}{\partial x} - \frac{\partial}{\partial x}\left(\epsilon^{ex4} D\frac{\partial c}{\partial x}\right) - \left(\frac{1 - 2t^\circ_+}{2\mathbf{F}}\right)(1 - c\bar{V}_e)\frac{\partial i_2}{\partial x} = 0 \quad [42]$$

electrode kinetics—

for discharge and rest

$$\frac{\partial i_2}{\partial x} - a_{max4} i_{o4,ref}\left(\frac{c}{c_{ref}}\right)^{\gamma 4}\left(\frac{\epsilon - \epsilon_{o4}}{\epsilon_{max4} - \epsilon_{o4}}\right)^{\zeta 4}\left\{\exp\left[\frac{\alpha_{a4}\mathbf{F}}{RT}(\phi_1 - \phi_2)\right] - \exp\left[\frac{-\alpha_{o4}\mathbf{F}}{RT}(\phi_1 - \phi_2)\right]\right\} = 0 \quad [43a]$$

and for charge

$$\frac{\partial i_2}{\partial x} - a_{max4} i_{o4,ref}\left(\frac{c}{c_{ref}}\right)^{\gamma 4}\left(\frac{\epsilon - \epsilon_{o4}}{\epsilon_{max4} - \epsilon_{o4}}\right)^{\zeta 4}\left(\frac{\epsilon_{max4} - \epsilon}{\epsilon_{max4} - \epsilon_{o4}}\right)\left\{\exp\left[\frac{\alpha_{a4}\mathbf{F}}{RT}(\phi_1 - \phi_2)\right] - \exp\left[\frac{-\alpha_{c4}\mathbf{F}}{RT}(\phi_1 - \phi_2)\right]\right\} = 0 \quad [43b]$$

Equations [39] through [43] are counterparts of the equations established for the positive electrode. The conceptual reference electrode used to measure the potential difference is a lead electrode, the same kind as the negative electrode.

Center of the negative electrode, $x = l$.—Equations [1], [2], [3], [5], and [43a] or [43b] apply. Since the electrode solid phase potential was set to zero at the other boundary ($x = 0$), a kinetic expression is used to calculate ϕ_1 at this boundary.

Numerical Procedure

The governing equations were put into finite difference forms and solved using the numerical technique of Newman (18, 19). The cell was divided into NJ node points with $J = 1$ designated to be the center of the positive electrode and $J = NJ$ to be the center of the negative electrode. Each region was evenly divided, but node point spacings were different between regions.

The finite difference approximations of the derivatives for an internal mesh point can be written as

$$\frac{\partial^2 C_k(J)}{\partial x^2} \simeq \frac{C_k(J+1) + C_k(J-1) - 2C_k(J)}{(\Delta x)^2} \quad [44]$$

$$\frac{\partial C_k(J)}{\partial x} \simeq \frac{C_k(J+1) - C_k(J-1)}{2(\Delta x)} \quad [45]$$

and for a boundary node

$$\frac{\partial C_k(J)}{\partial x} \simeq \frac{-C_k(J+2) + 4C_k(J+1) - 3C_k(J)}{2(\Delta x)} \quad [46]$$

$$\frac{\partial C_k(J)}{\partial x} \simeq \frac{C_k(J-2) - 4C_k(J-1) + 3C_k(J)}{2(\Delta x)} \quad [47]$$

where Δx denotes the distance between node points and $C_k(J)$ represents the k^{th} unknown at node J.

The accuracy of the finite difference approximations of the above derivatives is $(\Delta x)^2$. Equation [46], in the forward difference form, is used at $J = 1$; and Eq. [47], in the backward difference form, is used at $J = NJ$. for the internal boundaries, Eq. [46] is used on the higher region number side and Eq. [47] is used on the lower region number side. For example, Eq. [24] written in the finite difference form is

$$D\frac{C_1(J-2) - 4C_1(J-1) + 3C_1(J)}{2(\Delta x_2)} - C_1(J)v_2^{\blacksquare} = D\epsilon_{sep}^{ex3}\frac{-C_1(J+2) + 4C_1(J+1) - 3C_1(J)}{2(\Delta x_3)} - C_1(J)v_3^{\blacksquare} \quad [48]$$

where the electrolyte concentration c is written as "unknown 1". The subscript on Δx refers to the region number. We note that five node points are needed to describe the continuity of the flux at an internal boundary to maintain $(\Delta x)^2$ accuracy. Newman's BAND(J) can be used for only three node points (18, 19). Consequently, since up to five node points are used at an internal boundary, a modified version of Newman's subroutine, called Pentadiagonal BAND(J) (20, 21), was used instead. As the name implies, this subroutine allows up to five node points to be used at any position.

For the time derivative, implicit stepping was used

$$\frac{\partial C_k(J)}{\partial t} \simeq \frac{C_k(J) - CK_k(J)}{\Delta t} \quad [49]$$

where $CK_k(J)$ refers to the value at the previous time step, $t - \Delta t$. Initial distributions of variables can be determined by taking a small time step (10^{-4}s, *e.g.*).

Results and Discussion

In this section, we examine some simulated results and their implications. The parameters used in the calculations are given in Table I. Parameters not referenced are arbitrary but reasonable quantities. The same exchange current densities were assigned to the positive and negative electrodes. These values were chosen so that the calculated cell voltages agree well with measured ones.

Effect of temperature on discharge.—The simulated discharge behavior at 25° and −18°C under a constant current density of 340 mA/cm² is presented first. The discharge cutoff was chosen to be 1.55V. The temperature dependence of the kinetic expression is explicitly expressed in the exponential terms. Implicitly, the exchange current density in the kinetic expression is also a strong function of temperature. As mentioned earlier, the exchange current density was adjusted for the two temperatures so that the calculated cell voltages agreed relatively well with experimental observations.

Downloaded 13 Jun 2011 to 129.252.106.227. Redistribution subject to ECS license or copyright; see http://www.ecsdl.org/terms_use.jsp

Table I. Parameters used in the calculations

	Electrolyte
Acid concentration	4.9×10^{-3} mol/cm³ (1.280 sp gr)
Transference number	0.72 [Ref. (13), p. 78]
Partial molar volume of acid	45 cm³/mol [Ref. (11), p. 68]
Acid diffusion coefficient	3.02×10^{-5} cm²/s at 25°C [Ref. (16)]
Acid conductivity	0.79 S/cm at 25°C [Ref. (11), p. 74]
	Positive electrode
Number of node points	21
Half thickness of plate	0.06 or 0.03 cm
Maximum plate porosity	0.53 or 0.65
Maximum charge	5660 or 4615 C/cm³
Maximum specific surface area	100 cm²/cm³
Exchange current density	1.0×10^{-2} A/cm² at 25°C 2.0×10^{-3} A/cm² at −18°C
α_{a1}	0.5
α_{c1}	0.5
$\gamma 1$	1.5
$\zeta 1$	1.0
Lead dioxide conductivity	80 S/cm
ex1	1.5
exm1	0.5
	Reservoir
Number of node points	14
Thickness of reservoir	0.055 cm
	Separator
Number of node points	6
Thickness of separator	0.014 cm
Porosity	0.73
ex3	3.53
	Negative electrode
Number of node points	21
Half thickness of plate	0.06 or 0.03 cm
Maximum plate porosity	0.53 or 0.65
Maximum charge	5660 or 4615 C/cm³
Maximum specific surface area	100 cm²/cm³
Exchange current density	1.0×10^{-2} A/cm² at 25°C 2.0×10^{-3} A/cm² at −18°C
α_{a4}	0.5
α_{c4}	0.5
$\gamma 4$	1.5
$\zeta 4$	1.0
Lead conductivity	4.8×10^4 S/cm
ex4	1.5
exm4	0.5

The electrolyte conductivity and diffusion coefficient are also quite temperature dependent. They were calculated using the following equations

$$\kappa = \kappa_{25} \exp\left(\frac{1801}{298.15} - \frac{1801}{T}\right) \quad [50]$$

$$D = D_{25} \exp\left(\frac{2174}{298.15} - \frac{2174}{T}\right) \quad [51]$$

where κ and D are the conductivity and the diffusion coefficient of 1.280 sp gr H_2SO_4 at the absolute temperature, T; and κ_{25} and D_{25} are the conductivity and the diffusion coefficient at 25°C. The conductivity of the Pb or PbO_2 matrix has a weak temperature dependence and is assumed constant.

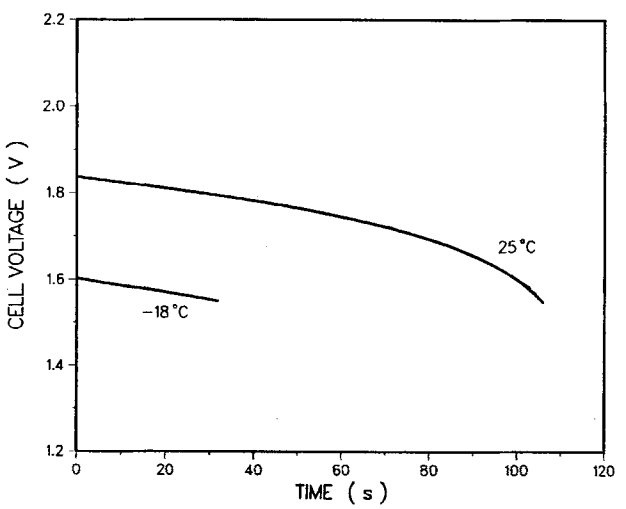

Fig. 2. Discharge cell voltage curves. 340 mA/cm²

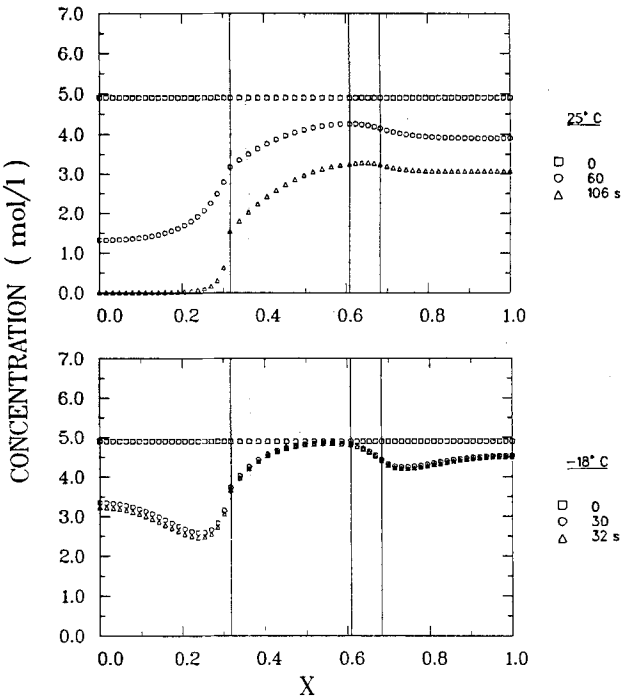

Fig. 3. Profiles of acid concentration during a discharge at 340 mA/cm². The regions from left to right are: positive electrode, reservoir, separator, and negative electrode. $X = 1.0$ is for $l = 0.19$ cm.

Cell voltage profiles during discharge are given in Fig. 2. The time to the voltage cutoff at 25°C is 106s and at −18°C is 32s. Acid concentration profiles (Fig. 3) show that the end of discharge at 25°C is caused by acid depletion in the positive electrode. At −18°C, ohmic and kinetic effects override the effect of acid depletion to cause the earlier discharge cutoff. The electrode capacity profiles (Fig. 4) indicate that for both cases, the electrodes are not very well utilized.

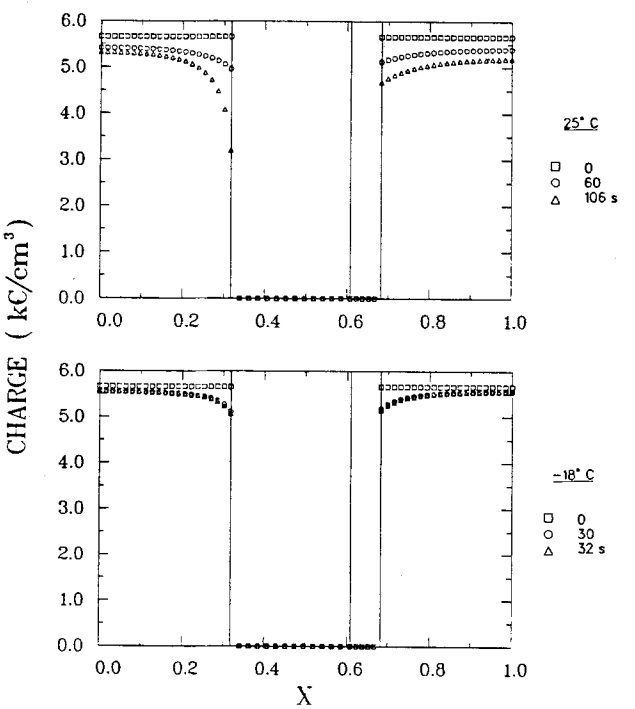

Fig. 4. Profiles of electrode capacity during a discharge at 340 mA/cm². The regions from left to right are: positive electrode, reservoir, separator, and negative electrode. $X = 1.0$ is for $l = 0.19$ cm.

Downloaded 13 Jun 2011 to 129.252.106.227. Redistribution subject to ECS license or copyright; see http://www.ecsdl.org/terms_use.jsp

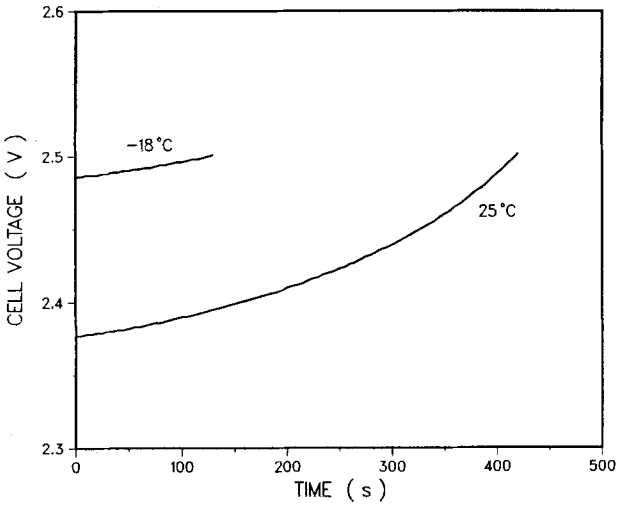

Fig. 5. Charge cell voltage curves. 20 mA/cm²

Effect of temperature on charge.—Charge behavior was simulated at 25° and −18°C under a constant charge current density of 20 mA/cm² and a voltage cutoff of 2.5V. The simulations were based on a previous discharge at −18°C and 340 mA/cm² to a cutoff of 1.55V, and a rest period of 1h at −18°C.

Figure 5 shows the cell voltage profiles during charge at the two temperatures. By charging the cell at 25°C, we can put about 223% more charge into the cell. At −18°C, constant current charging is inefficient because of a penalty of more than 0.1V at the very beginning of the charge.

The concentration profiles for the two cases are shown in Fig. 6. Note that the concentration of the electrolyte has not totally relaxed at the end of the 1h rest. This is an indication of the sluggish diffusion of the species when the operating temperature is low. The charge profiles in Fig. 7 show the nonuniform distribution of charge across the electrodes.

We should mention that in practice, the lead-acid battery is charged under a constant potential with a current limit. This charging condition can also be simulated by the present model by iterating on the applied charging current.

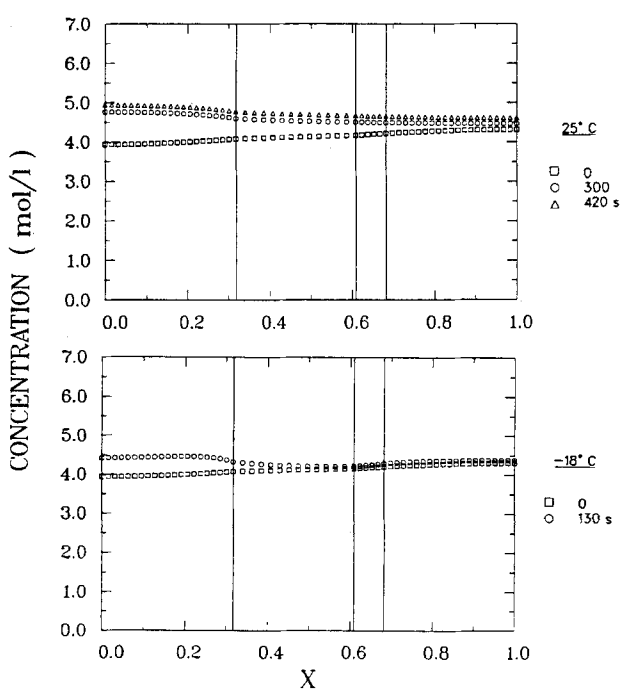

Fig. 6. Profiles of acid concentration during a charge at 20 mA/cm². The regions from left to right are: positive electrode, reservoir, separator, and negative electrode. $X = 1.0$ is for $l = 0.19$ cm.

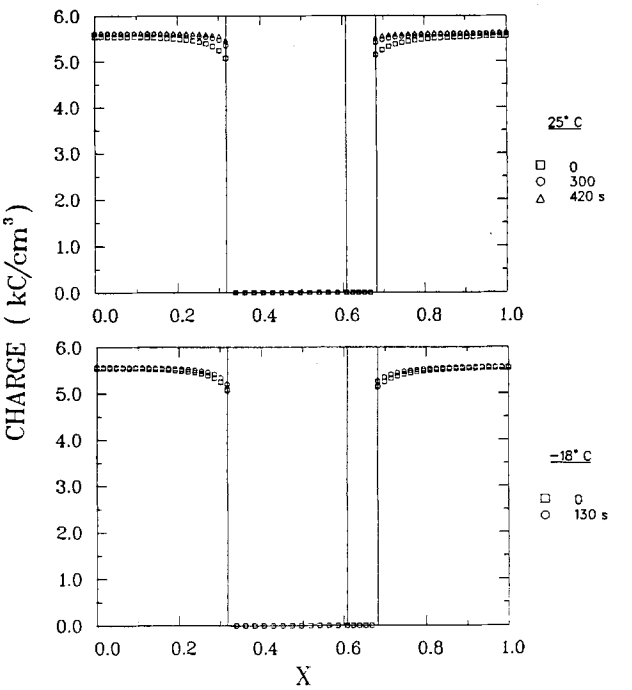

Fig. 7. Profiles of electrode capacity during a charge at 20 mA/cm². The regions from left to right are: positive electrode, reservoir, separator, and negative electrode. $X = 1.0$ is for $l = 0.19$ cm.

Effect of electrode thickness.—The simulations reported so far have been for 0.12 cm thick electrodes. Next, the effects of using either a 0.06 cm thick positive or a 0.06 cm thick negative will be examined. As shown in Fig. 8, a thin positive electrode has a greater effect on the cell voltage. The discharge time to 1.55V for: (a) two thick electrodes, (b) one thick positive and one thin negative, and (c) one thin positive and one thick negative are 32, 22, and 17s, respectively.

The same kinetic parameters were used for the positive and negative electrodes in the simulations. The only differences between the two electrodes are the solid phase conductivity and the electrode reaction. The solid phase conductivity does not have much influence on the electrode behavior when an electrode is thin. Consequently, there is no observable difference between case b and case c initially. With time, however, case c shows a steeper drop in cell voltage. This is because the amount of electrolyte supply is important to the positive electrode reaction. A thinner positive electrode contains less acid in its pores. A thin positive electrode will polarize more quickly than a thin negative electrode due to the

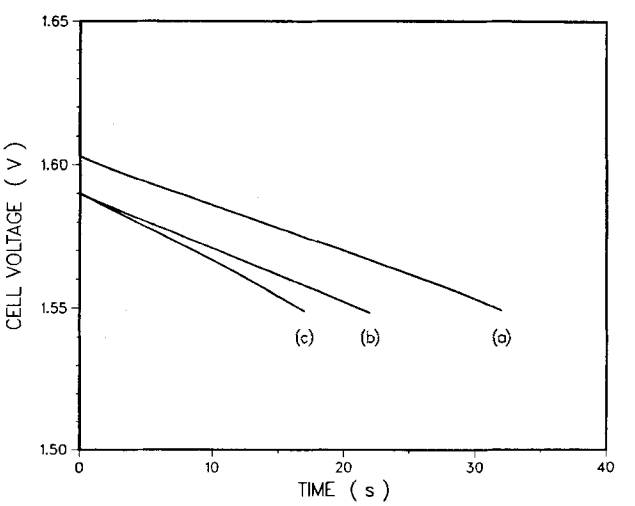

Fig. 8. Discharge cell voltage curves for (a) two thick electrodes, (b) one thick positive and one thin negative, and (c) one thin positive and one thick negative. 340 mA/cm² and −18°C.

Downloaded 13 Jun 2011 to 129.252.106.227. Redistribution subject to ECS license or copyright; see http://www.ecsdl.org/terms_use.jsp

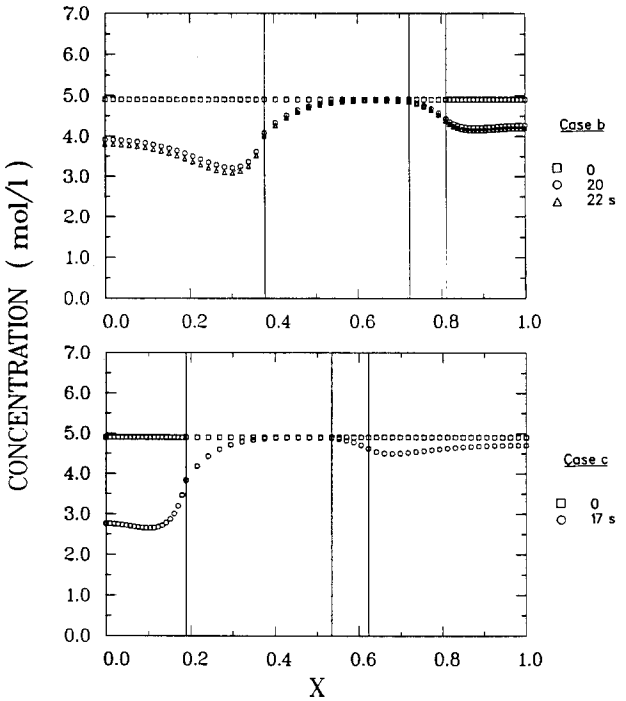

Fig. 9. Profiles of electrolyte concentration during a discharge. 340 mA/cm² and −18°C. $X = 1.0$ is for $l = 0.16$ cm.

depletion of the acid supply. The electrolyte concentration profiles for case b and case c are shown in Fig. 9.

Effect of porosity.—The simulations have been based so far on both electrodes having an initial porosity of 0.53. Next, the effect of having a larger initial porosity of 0.65, one electrode at a time will be examined. The electrodes are 0.12 cm thick. The discharge cell voltage curves are shown in Fig. 10 for (a) both electrodes having an initial porosity of 0.53, (b) a porosity of 0.53 in the positive electrode and a porosity of 0.65 in the negative electrode, and (c) a porosity of 0.65 in the positive electrode and a porosity of 0.53 in the negative electrode. Increasing the porosity of either electrode increases the discharge time. The porosity of the positive electrode, however, has a greater effect on the discharge behavior. This is again related to the acid availability near the reaction sites inside the positive electrode.

Conclusions

A mathematical model of a lead-acid cell has been presented. This model predicts profiles of acid concentration, overpotential, porosity, reaction rate, and electrode capacity as functions of time and temperature. Cell behavior during discharge, rest, and charge can be simulated.

The model can be used to evaluate the effects of electrode porosity, electrode thickness, various separators, acid reservoir volume, and operating temperature on the performance of the cell (voltage, power, and cold cranking amperage). With reasonably assumed parameters, under constant current charge or discharge conditions, it is concluded that:

1. Discharge at room temperature to a cell voltage cutoff of 1.55V is limited by the acid in the positive electrode. However, at a low temperature such as −18°C, the slow kinetics, diffusion, and high ohmic losses are enough to drive the cell voltage to the cutoff even before acid depletion sets in.

2. Charge at a low temperature is inefficient because of the same factors limiting a low temperature discharge. A voltage premium of 0.1V is needed in order to overcome the various losses at the onset of a 20 mA/cm² charge.

3. It is better to store the electrolyte in the pores of the positive electrode instead of in an external reservoir. For a discharge at −18°C under a current density of 340 mA/cm², the discharge time to 1.55V is increased by 11s

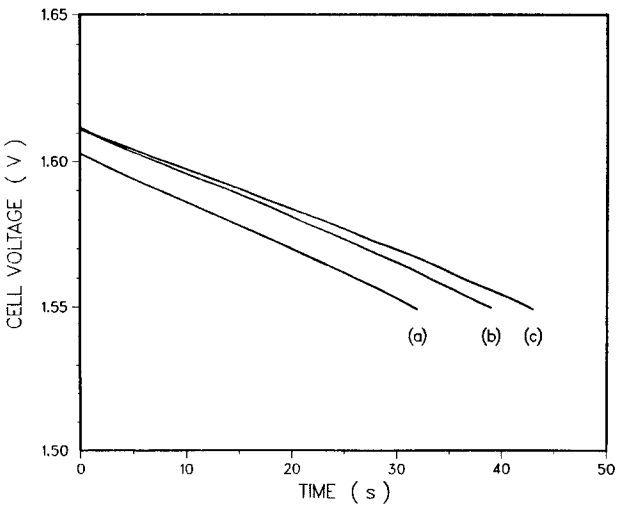

Fig. 10. Discharge cell voltage profiles for (a) both electrodes 0.53 initial porosity, (b) positive 0.53 and negative 0.65, and (c) positive 0.65 and negative 0.53. 340 mA/cm² and −18°C.

when a positive electrode with 0.53 initial porosity is replaced by one with 0.65 initial porosity.

4. A negative electrode with 0.65 initial porosity instead of 0.53 also improves the discharge time by 7s. This improvement is due mainly to a reduction in ohmic losses in the electrode pores.

5. A thin electrode increases the polarization of a cell because a higher current density is realized due to the reduction in the reaction surface area. A thin positive electrode is polarized even faster because of the reduced volume of acid in the electrode.

Acknowledgment

The authors wish to thank General Motors Research Laboratories and Delco-Remy Division for support of this work and for permission to publish this article.

Manuscript received Jan. 12, 1987.

The General Motors Research Laboratories assisted in meeting the publication costs of this article.

LIST OF SYMBOLS

a_{max1}	maximum specific active surface area in region 1, cm²/cm³
a_{max4}	maximum specific active surface area in region 4, cm²/cm³
c	concentration of the binary electrolyte, mol/cm³
c_i	concentration of species i, mol/cm³
c_{ref}	reference concentration of the binary electrolyte, mol/cm³
D	diffusion coefficient of the binary electrolyte, cm²/s
ex1, exm1	exponents on porosity in region 1
ex3	exponent on porosity in region 3
ex4, exm4	exponents on porosity in region 4
f	mean molar activity coefficient
$\mathbf{F}$	Faraday's constant, 96,487 C/mol
$i_{o1,ref}$	exchange current density at c_{ref} for the positive electrode, A/cm²
$i_{o4,ref}$	exchange current density at c_{ref} for the negative electrode, A/cm²
i_2	superficial current density in the solution based on projected electrode area, A/cm²
I	total applied current density based on projected electrode area, A/cm²
j	reaction current per unit volume of electrode, A/cm³
l	distance between positive and negative electrode current collectors, cm
MW_i	molecular weight of species i (i = $PbSO_4$, PbO_2, Pb), g/mol
n	number of electrons involved in electrode reaction
N_i	flux of species i, mol, mol/cm²-s
R	universal gas constant, 8.3143 J/mol-K
t	time, s
t°_+	transference number of H^+ with respect to the solvent velocity

Downloaded 13 Jun 2011 to 129.252.106.227. Redistribution subject to ECS license or copyright; see http://www.ecsdl.org/terms_use.jsp

T	absolute temperature, K
U_{Pb}^{θ}, $U_{PbO_2}^{\theta}$	standard electrode potentials referred to the hydrogen electrode
U_{PbO_2}	rest-potential difference between PbO_2 and Pb electrodes
v_i	velocity of species i, cm/s
$v^{\blacksquare}$	volume-average velocity, cm/s
$v_1^{\blacksquare}$, $v_2^{\blacksquare}$, $v_3^{\blacksquare}$, $v_4^{\blacksquare}$	volume-average velocity in regions 1, 2, 3, and 4, cm/s
V_i	partial molar volume of species i, cm^3/mol
x	distance from the center of the positive electrode, cm
X	the ratio of x to the total cell thickness (half electrodes)

Greek letters

α_{a1}, α_{c1}	anodic and cathodic transfer coefficients for the positive electrode
α_{a4}, α_{c4}	anodic and cathodic transfer coefficients for the negative electrode
$\gamma 1$, $\gamma 4$	exponents for the concentration dependence of the exchange current density
ϵ	porosity
ϵ_{o1}, ϵ_{o4}	porosities at zero charge for the positive and negative electrodes
ϵ_{sep}	porosity of the separator
ϵ_{max1}, ϵ_{max4}	porosities at fully charged state of the positive and negative electrodes
$\zeta 1$, $\zeta 4$	exponents for the charge dependence of the specific active surface area
κ	electrolyte conductivity, S/cm
ρ_i	density of species i (i = $PbSO_4$, PbO_2, Pb), g/cm^3
σ_i	conductivity of the electrode solid phase (i = Pb, PbO_2), S/cm
ϕ_1	potential in the electrode matrix, V
ϕ_2	potential in the solution, V

Subscripts

e	electrolyte
o	solvent
+	cation
−	anion

REFERENCES

1. D. Pletcher, "Industrial Electrochemistry," Chapman and Hall, New York (1982).
2. W. Stein, *Naturwissenschaften*, **45**, 459 (1958).
3. W. Stein, Ph.D. Thesis, Rheinisch-Westfalischen Techn. Hochschule Aachen, Aachen, Germany (1959).
4. J. Euler, *Electrochim. Acta*, **4**, 27 (1961).
5. D. Simonsson, *This Journal*, **120**, 151 (1973)
6. D. Simonsson, *J. Appl. Electrochem.*, **3**, 261 (1973).
7. D. Simonsson, Dissertation, Inst. Kemisk Teknologi, Kungl. Tekniska Hogskolan, Stockholm, Sweden (1973).
8. K. Micka and I. Rousar, *Electrochim. Acta*, **18**, 629 (1973).
9. D. Gidaspow and B. Baker, *This Journal*, **120**, 1005 (1973).
10. J. Newman and W. H. Tiedemann, *AIChE J.*, **21**, 25 (1975).
11. W. H. Tiedemann and J. Newman, in "Battery Design and Optimization," S. Gross, Editor, p. 23, The Electrochemical Society Softbound Proceedings Series, Princeton, NJ (1979).
12. W. S. Sunu, in "Electrochemical Cell Design," R. E. White, Editor, p. 357, Plenum Press, New York (1984).
13. J. S. Dunning, Ph.D. Dissertation, University of California, Los Angeles, CA (1971).
14. J. A. Trainham, Ph.D. Dissertation, University of California, Berkeley, CA (1979).
15. R. B. Bird, W. E. Stewart, and E. N. Lightfoot, "Transport Phenomena," John Wiley & Sons, Inc., New York (1960).
16. R. Pollard and J. Newman, *This Journal*, **128**, 491 (1981).
17. K. C. Tsaur and R. Pollard, *ibid.*, **131**, 975 (1984).
18. J. Newman, *Ind. Eng. Chem. Fundam.*, **7**, 514 (1968).
19. J. Newman, "Electrochemical Systems," Prentice-Hall, Inc., Englewood Cliffs, NJ (1973).
20. R. White, C. M. Mohr, P. Fedkiw, and J. Newman, LBL-3910, Lawrence Berkeley Laboratory, University of California, Berkeley, CA (1975).
21. J. Van Zee, G. Kleine, R. E. White, and J. Newman, "Electrochemical Cell Design," R. E. White, Editor, Plenum Press, New York (1984).

Electrochemical Behavior of Some Lead Alloys

M. N. C. Ijomah

Department of Metallurgy and Materials Engineering, Anambra State University of Technology, P. M. B. 01660, Enugu, Nigeria

ABSTRACT

A series of lead alloy specimens comprising binary Pb-Li, Pb-Sn, Pb-Sb, and quinary Pb-(Al, Mg, Sn, Li) alloys were electrochemically tested. The corrosion cell was set up in 30% H_2SO_4, using a mercury-mercurous sulfate reference electrode. The passivity subsequently attained by the respective alloys depended primarily upon the presence of a nonconducting $PbSO_4$ film, the morphology (solubility, porosity, and strength of adhesion) of which depended, to a great extent, upon the nature and concentration of the various alloying elements. The influence of tin and antimony were clearly dominant and they played contrasting roles during actual passivation. Corrosion was associated with the preferential attack of the grain boundary regions since segregation of alloying elements at the grain boundaries provided the metal with a built-in electrochemical cell. Homogeneous or single-phase alloys corroded uniformly and recorded similar behavior to pure lead while the richer alloys suffered severe intergranular corrosion and were anomalous. The above findings were conveniently supported with both scanning electron microscopy and electron probe microanalysis and implications in the lead-acid battery technology were effectively discussed.

The electrochemical behavior of lead in sulfuric acid had been extensively studied (1-12, 18, 23, 26-31, 40-45). When lead is polarized in sulfuric acid solution in the potential range between hydrogen and oxygen evolution, a number of electrochemical reactions occur (see Table I), two of which represent the charge and discharge reactions of the lead acid battery, namely

$$Pb + SO_4^{2-} \underset{c}{\overset{d}{\rightleftharpoons}} PbSO_4 + 2e \ (E^\circ = -0.356V)$$

$$PbO_2 + SO_4^{2-} + 4H^+ + 2e \underset{c}{\overset{d}{\rightleftharpoons}} PbSO_4 + 2H_2O \ (E^\circ = 1.685V)$$

The passivity subsequently attained apparently resulted from the presence of a virtually insoluble and nonconducting lead sulfate film on the electrode surface. It had been claimed that intermediate compounds (basic sulfates, lead monoxide, etc.) tended to form underneath the lead sulfate film and that oxygen evolution occurred after conversion of the lead sulfate to a polymorphic lead dioxide film (2, 6-8, 18, 41, 43). The electrochemical behavior of lead in sulfuric acid has obvious implication in the lead-acid battery, the performance of which depends, to a great extent, upon the type of lead alloy employed as a grid. Although the grid metal does not participate directly in primary charge and discharge processes, it often limits the life and utility of the battery. Corrosion and disintegration of the positive grid is the prime reason for

Downloaded 13 Jun 2011 to 129.252.106.227. Redistribution subject to ECS license or copyright; see http://www.ecsdl.org/terms_use.jsp